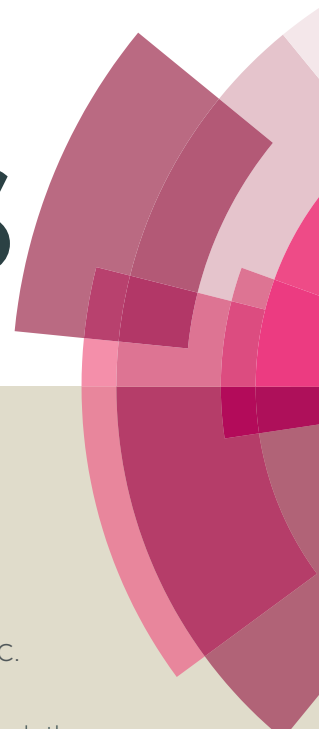


RSC Advances



This article can be cited before page numbers have been issued, to do this please use: J. Zhou, R. Xu, C. Yin, Z. Li, W. Wu and M. Wu, *RSC Adv.*, 2016, DOI: 10.1039/C6RA11597G.



This is an *Accepted Manuscript*, which has been through the Royal Society of Chemistry peer review process and has been accepted for publication.

Accepted Manuscripts are published online shortly after acceptance, before technical editing, formatting and proof reading. Using this free service, authors can make their results available to the community, in citable form, before we publish the edited article. This *Accepted Manuscript* will be replaced by the edited, formatted and paginated article as soon as this is available.

You can find more information about *Accepted Manuscripts* in the [Information for Authors](#).

Please note that technical editing may introduce minor changes to the text and/or graphics, which may alter content. The journal's standard [Terms & Conditions](#) and the [Ethical guidelines](#) still apply. In no event shall the Royal Society of Chemistry be held responsible for any errors or omissions in this *Accepted Manuscript* or any consequences arising from the use of any information it contains.



Journal Name

ARTICLE

In-situ Grown of Polyphosphazene Nanoparticles on Graphene sheets as Highly Stable Nanocomposite for Metal-Free Lithium Anode

Jingyan Zhou, Rongfei Xu, Changzhi Yin, Zhongtao Li,* Wenting Wu, Mingbo Wu*

Received 00th January 20xx,
Accepted 00th January 20xx

DOI: 10.1039/x0xx00000x

www.rsc.org/

A polyphosphazene/GN nano-composite was readily synthesized by thermal polymerization of hexachlorocyclotriphosphazene with graphene oxide, which exhibits stable and uniform nanostructure. The introduction of electronic-withdrawing polyphosphazene nanoparticles on graphene could effectively create a great number of active sites and avoid the stacking of aromatic layers of graphene, which attributes to providing more domains for lithium storage and accelerating charge transformability. Therefore, an excellent rechargeable capability (1002 mAh g^{-1} at 100 mA g^{-1}) and rate performance (321 mAh g^{-1} at 5 A g^{-1}) as metal-free Li-ion batteries anode could be achieved.

1. Introduction

With the increasing demands on power supplier for portable electronic devices and powering electric vehicles in the modern society, high energy density, long cycle life, as well as high rate performance of lithium-ion batteries (LIBs) are essential and extensively used^[1-6]. Graphite, the most commonly used commercial anode material in LIBs, has excellent cycling stability and low cost. But, bulk graphite can react with Li to form LiC_6 structures with a lower specific capacity of 372 mAh g^{-1} , which significantly limits the specific energy and rate performance of LIBs.^[7] Therefore, intense efforts have been focused to searching for new carbon based anode materials with enhanced Li^+ ion storage capacity, which are more economic and environment friendly other than metal oxide anodes.^[8]

The intentional incorporation of heteroatoms onto graphene could modify the electronic and crystalline structures and further effectively change its electronic and chemical properties.^[9,10] Recently, phosphorus, sulphur, boron, nitrogen^[11-13] have been used as dopants to improve the electrochemical performance of carbon materials. The doping of such atoms breaks the electroneutrality of the graphene and creates charged sites, which is beneficial to the enhancement of electrochemical conductivity and Li^+ ion accommodation^[14,15]. For instance, due to the higher

electronegativity of N and smaller atomic diameter in comparison to carbon, the stronger interaction between the nitrogen-modified carbon material and lithium might be favourable for lithium insertion. Besides, the incorporation of N containing domain onto the carbon matrix can generate n-type conductive material, wherein N introduces donor states near Fermi level.^[16, 17] P and N are in the same main group, whereas P has higher electron-coordination ability and exhibits stronger n-type behaviours. Recently, Cho et al.^[18] studied the effect of these two nitrogen-doped structures on the charge capacity of the LIBs. They found that N doped graphene on silver-assisted chemically etched Si nanowires increases the capacity of Li intercalation by forming vacancies and dangling bonds around the N dopants. Zhang^[19] prepared P-modified graphene by a thermal treatment using graphene oxide and triphenylphosphine, which significantly improved the electrochemical properties in oxygen reduction reaction (ORR) and lithium ion batteries (LIB). Ma and co-workers^[20] developed a facile one-step CVD approach to synthesize the P and N dual-doped nano-mesh graphene through an in situ doping process, which lead to an extraordinary electrochemical performance as anodes in LIBs.

The inorganic conjugated compound, namely hexachlorocyclotriphosphazene (HCCP), which is the precursor of polyphosphazene nanoparticles (PPN), is composed of s-triazine-like P-N heterocyclic ring. The unique structure of HCCP render to some special properties, like high anti-flammability and strong electro-withdrawing effect. Therefore, some electronic materials that contain triphosphazene subunits have been reported. Xu^[21] prepared novel inorganic network polymer phosphazene disulfide $[(\text{NPS}_2)_3]_n$ by a solution cross-link method, its unique composition and molecular structure, making the polymer has a non-flammable

State Key Laboratory of Heavy Oil Processing, China University of Petroleum, Qingdao 266580, China.

*Corresponding Author: E-mail: liztao@upc.edu.cn, Tel: +86532-86984615; wumb@upc.edu.cn

† Footnotes relating to the title and/or authors should appear here.

Electronic Supplementary Information (ESI) available: [Additional experimental data including BET surface, N_2 adsorption/desorption isotherms, FT-IR patterns, Elemental composition]. See DOI: 10.1039/x0xx00000x

and superior electrical conductivity. Dufek^[22] reported a new kind of cyclic phosphazenes/graphene as anode for LIBs, which was synthesized as a result of chemical reaction between methyl hydroquinone cyclophosphazene (MeHQCP) or tert-butyl hydroquinone cyclophosphazene (tbu-HQCP) and graphene, and improving the cycle stability and safety of the electrode.

Herein, we utilized HCCP as P and N source to modify graphene oxide sheets. The HCCP could react with GO and polymerize with each other on the GO sheets during high temperature thermal processing, through which the defects/disorders and N, P atoms are readily introduced onto GO sheets to prepare well-dispersed nanocomposite. The introducing N, P could effectively create a great number of active sites on graphene and avoid the stacking of aromatic planes, which effectively contribute to providing more lithium ions storage regions, enhancing the electronic conductivity and iron transformability.

2. Experimental Section

2.1 Materials preparation

Hexachlorocyclotriphosphazene (HCCP) (Aldrich) was recrystallized from dry hexane followed by sublimation (60 °C) twice before use^[23]. All other materials from Aladdin Chemical Regents were of analytical grade and used without any further purification.

Preparation of Polyphosphazene Nanoparticles/graphene (PPN/GN)

Graphite oxide (GO) was synthesized from graphite powder by a modified Hummers' method.^[24-26]

Graphite oxide (500 mg) was exfoliated in ethyl alcohol absolute (500 mL) with ultrasonic treatment (700 W, 2 h) to form a colloidal suspension, and the resultant suspension is marked as solution A. Hexachlorocyclotriphosphazene (50 mg) was dissolved in 20 mL tetrahydrofuran (THF) to form homogeneous solution B. And then solution B is gradually added into solution A with stirring, the mixture was heated to 65°C and allowed to react for 1h. After evaporation of ethanol and tetrahydrofuran, the obtained GO/HCCP mixture was dried in a vacuum oven at 70°C overnight. The annealing treatment was then carried out in a tube furnace with flowing nitrogen as protective ambient. The resulting mixture was put in a quartz boat in the center of a tube furnace and annealed at the designed temperature (700°C) for 3 h. The product PPN/GN was collected when the furnace temperature was below 60°C.^[19]

As a control sample, Graphite oxide was treated throughout the whole processes as mentioned above to prepare the sample as GN, except the introduction of HCCP.

2.2 Analysis instruments

The chemical structures of the samples were characterized by Fourier transform infrared spectrometry (FTIR, Thermo Nicolet NEXUS 670, USA). X-ray photoelectron spectroscopy (XPS, Thermo Scientific ESCALab250Xi, AlK α) was used to characterize chemical structure in future. The XRD pattern of the polyimides was recorded on an X'Pert PRO MPD X-ray diffractometer equipped with a monochromatized Cu K α radiation from 10-75°. The stabilization of monomer and polymer were determined by thermogravimetric analysis (TGA, Netzsch STA 449C, Germany).

2.3 Samples characterization

The morphologies of obtained samples were investigated using field emission scanning electron microscopy (SEM, Hitachi S-4800, Japan), transmission electron microscopy (TEM, JEM-2100UHR, Japan) and X-ray powder diffraction (XRD) using an X-ray diffractometer with Cu K α radiation from 10-75°. Raman analysis was performed on a Jobin Yvon HR800 Raman spectrometer. Nitrogen adsorption-desorption isotherms were carried out on ASAP 2020 Micromeritics instrument. X-ray photoelectron spectroscopy (XPS) was performed on Thermo ESCALAB 250XI with a monochromatic Al K X-ray source.

2.4 Electrochemical measurement

Lithium ion batteries (LIBs) measurements were performed in two electrode cells using a LAND CT2001A electrochemical workstation. The working electrode was composed of active material, conductive agent (acetylene black) and a polyvinylidene fluoride binder in a weight ratio of 70:15:15 were mixed in N-methyl-2-pyrrolidone to obtain slurry. The slurry was spread onto a copper foil and then dried in a vacuum oven at 100 °C for 10 h to remove solvent. The electrodes were cut to disks typically with a diameter of ~12 mm, and the active materials average mass loading within the coin cells are around 1.0 mg for GN and PPN/GN. The cells were assembled in an argon-filled glove box, using lithium foil as the counter and reference electrode, a Celgard 2300 membrane separator, and 1 M LiPF₆ solution dissolved in 1:1 (v/v) mixture of ethylene carbonate (EC) and dimethyl carbonate (DMC). The charge and discharge were conducted on a battery test system at 25 °C at the current densities from 100 to 5000 mA g⁻¹ between 0.005 and 3 V vs Li⁺/Li at room temperature. Cyclic voltammograms (CV) were performed using an Ametek PARSTAT4000 electrochemistry workstation at a scan rate of 0.25 mV s⁻¹ within the potential range of 0.005–3 V.

3. Results and discussion

3.1 Structural characterization of materials

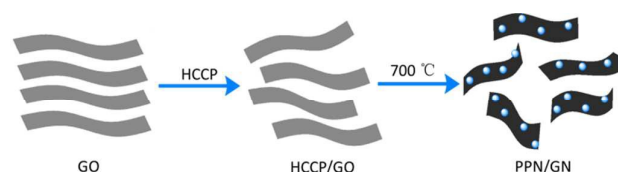


Fig. 1 The synthesis strategy of PPN/GN

The synthesis strategy of PPN/GN was illustrated in Figure 1. In the first, GO was prepared through a modified Hummers method. Then, the GO were mixed with the solution of HCCP in THF to form homogeneous suspension. After evaporation of solvents, the mixture was carbonized at 700°C for 3 hours with the protection of N₂. The chlorine in HCCP would react with hydrogen in GO to form HCl and expel out into atmosphere; then polymerized with each other through ring-opening of HCCP P-N heterocyclics, simultaneously. Thereafter, the polymerized PPN were firmly combined with GO via covalent bonds to form well-dispersed nanoparticle on GO layers and afford active region for Lithium ions coordination.

Fig. 2a shows the scanning electron microscopy (SEM) image of PPN/GN. The image reveals transparent graphene sheets with

wrinkle and fold features, which may originate from defective structures formed during reduction process of GO and HCCP. Furthermore, the polyphosphazene nanoparticles (yellow dots in figure 2a) on GO sheet which formed by thermal polymerization can be easily identified, and the average size is 15 nm. Fig. 2c, 2d represent the TEM elemental mappings of element P and N, which reveal the polyphosphazene nanoparticles (formed during thermal treatment of HCCP)^[27] are homogeneously distributed on the plane of graphene^[28]. The N₂ absorption isotherms for the as-prepared samples were shown in Fig. S1. The BET surface of the PPN/GN was 443.6 m² g⁻¹, larger than that of GN (342.9 m² g⁻¹) (Tab. S1). The doping of polyphosphazene nanoparticles seem increased the roughness of the composition, which would due to the firmly combination of polyphosphazene nanoparticles and avoiding of π - π stacking between graphene layers (also have been approved by SEM and TEM images in Fig. 2a and 2b).

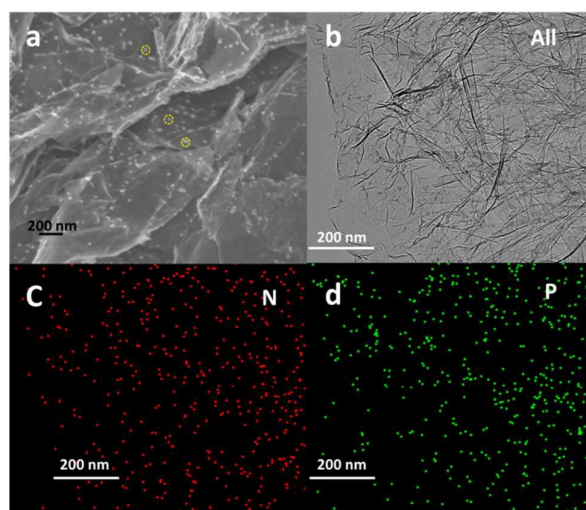


Fig. 2 (a) Scanning electron microscope (SEM), (b) transmission electron microscope (TEM) images, and (c, d) EDS elemental mapping of PPN/GN.

XPS analysis was carried out to determine the doping levels and bonding configurations of polyphosphazene on graphene nanosheets. The survey spectrum given in Fig. 3a shows three characteristic peaks at ca. 133, 285 and 400 eV, corresponding to the P 2p, C 1s and N 1s, respectively. Fig. 3c is the high resolution P 2p XPS spectrum of PPN/GN. The P 2p peak can be as LIBs anode. into two peaks at binding energies of ~133.5 and ~135 eV, which correspond to the P-O and P=N energy positions, respectively.^[27] Furthermore, increasing content of P-O is ascribed to the nucleophile substitution reaction between HCCP and GO. The N 1s peak (Fig. 3b) can be deconvoluted into three different peaks at binding energies of 398.4, 400.1 and 401.7 eV, which correspond to pyridinic-N, pyrrolic-N and graphitic-N,^[29] respectively. The doping levels

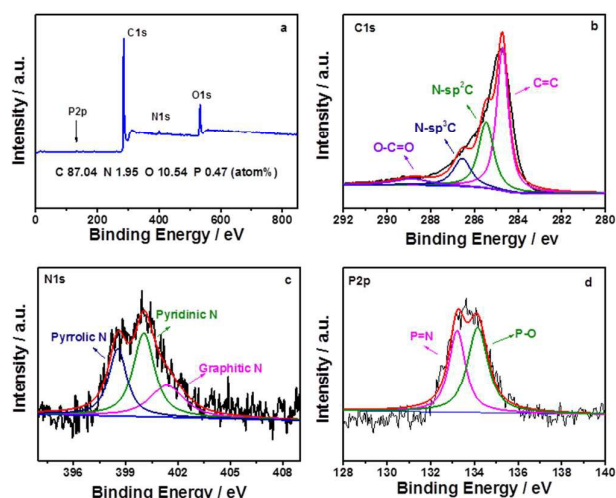


Fig. 3 XPS spectra of PPN/GN (a), the C 1s (b), the N 1s (c), and the P 2p (d)

of P and N in PPN/GN measured by XPS are 0.47 and 1.95 at %, respectively. The O content of PPN/GN is 10.54 at% (Tab. S2), which is much lower than that of the GO, indicating the deoxygenating of GO and the formation of the graphene structure during PPN modification, which could achieve higher the electrical conductivity. Figure 3b reveals that the C 1s peak can be well identified into four components at binding energies of 284.7 (C=C), 285.5 (N-sp²C), 287.7 (N-sp³C) and 288.4 eV (O-C=O). There is an obviously decrease in the epoxy group content of PPN/GN compared with that of GO, which also indicated increased content of the graphitic carbon in PPN/GN during thermal reduction.

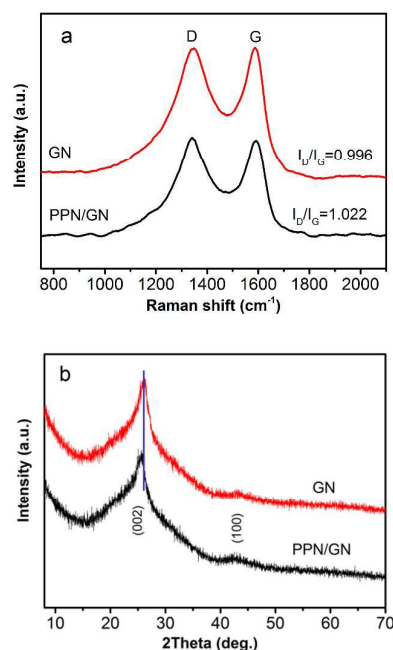


Fig. 4 (a) Raman spectra of PPN/GN and GN, (b) XRD patterns of PPN/GN and GN

To further understanding the chemical bonding between PPN/GN and GO, the FT-IR spectra of the two materials are compared and shown in Fig. S2. The peaks at 1725 and 1614 cm^{-1} in GO ascribe to the C=O stretching vibration and O-H deformation vibration in COOH groups.^[30,31] The intensity of the peaks become much smaller, suggesting that most COOH groups in GN are decomposed after calcination. It should be noted that the epoxy group peak of GN at 1225 cm^{-1} is largely reduced compared with that of GO.

Raman spectroscopy was carried out to evaluate the degree of structural deformations in GO and PPN/GN. As shown in Fig. 4a, two distinct peaks are attributed to the D band at ca. 1335 cm^{-1} and the G band at ca. 1590 cm^{-1} , respectively. The D band is commonly associated with a series of structural defects, whereas the G band is observed for all graphitic structures due to the first-order scattering of the E 2g mode^[19]. The intensity ratio of D band to G band (I_D/I_G) represents the disorder degree of graphene. In addition, Fig. 4a also shows that the intensity ratio of the D-band to the G-band (I_D/I_G) increases from GN (0.996) to PPN/GN (1.022), indicating that more defects or disorders were introduced into PPN/GN during the combination process. Because the Raman analysis could not accurately elucidate the graphitization degree of the composited sample, X-ray diffraction (XRD) analysis was conducted. Fig. 4b shows the XRD patterns of GN and PPN/GN. From the profile of PPN/GN, a well-defined peak at $2\theta = 25.8^\circ$ as that in GN could be found after annealing, which suggest the successful reduction of GO to graphene with a enforced graphitic crystalline structure.

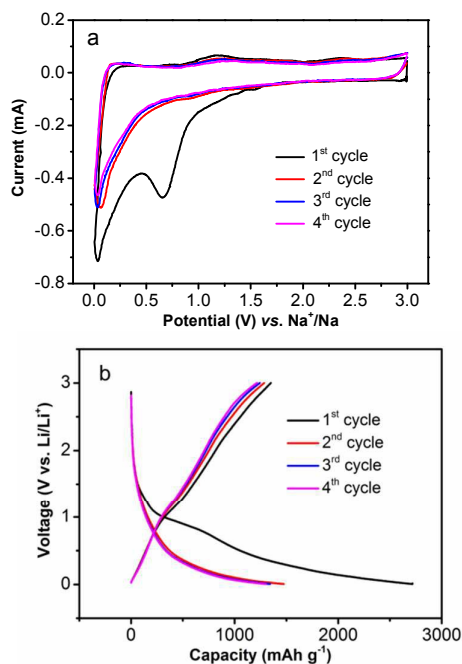


Fig.5 (a) CV curves of PPN/GN at a scanning rate of 0.2 mV s^{-1} , (b) Galvanostatic charge-discharge profile of PPN/GN at a current rate of 0.1 A g^{-1} .

3.2 Electrochemical characterization of materials

As shown in Fig. 5a, the initial four CV curves of the PPN/GN electrodes in the range of 0.005-3 V at a scan rate of 0.1 mV s^{-1} have been tested. The galvanostatic charge-discharge profile of the PPN/GN is shown in Fig. 5b. From Fig. 5a, the electrode exhibit two apparent peaks at 0.7 V and 1.5 V in the first reduction process. The peak at 0.7 V corresponds to the electrolyte decomposition and the formation of the solid electrolyte interphase (SEI) layer due to the presence of some functional groups on the PPN/GN surface and the plateau disappeared in the subsequent cycles.^[32, 33] The peak at 1.5 V can be observed in the subsequent curves indicate that lithium could be reversibly inserted into and extracted from the graphene layers. This result is in accordance with the voltage versus capacity profiles in Fig. 5b.

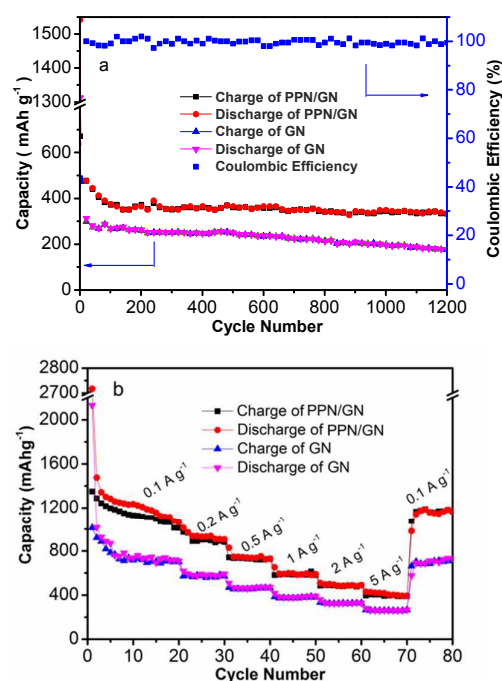


Fig. 6 (a) Long-term cycling performance of PPN/GN and GN at 5 A g^{-1} , (b) Rate capabilities of PPN/GN, GN electrodes at different current densities.

In Fig. 6a, the long-term cycling stability of GN and PPN/GN at a current density of 5 A g^{-1} are compared and the coulombic efficiency of PPN/GN are shown. As revealed in Fig. 6a, the PPN/GN anode exhibits excellent cycling stability. The reversible charge capacity still keeps at 321 mAh g^{-1} even after 1200 cycles. However, after 1200 cycles at the same current density, the capacity of reduced GN just kept at 218 mAh g^{-1} . The coulombic efficiency of PPN/GN at first cycle is 43.5%, then keeps stable 100% until 1200 cycles. The significantly improved electrochemical performance of PPN/GN is likely to be benefited from introduction of polyphosphazene nanoparticles: 1. The higher electron-coordination capability and stronger n-type behaviors of polyphosphazene

nanoparticles afford more active sites for lithium storage; 2. Increased the roughness of the PPN-GO composite would well separate the staking between graphene layers^[34], which could fabricate high conductive framework to accelerate charges and lithium ions transfer during cycling; 3. The high molecular weight polyphosphazene nanoparticles firmly bonded on GN sheets through covalent bonds, which could effectively avoid the dissolution of active materials from electrode into electrolyte during cycling.^[35] The rate capabilities of PPN/GN and GN at various lithiation/delithiation rates are presented in Fig. 6b. It is clear to see that PPN/GN exhibited a moderate capacity (1003, 953, 780, 600, 508, 456 mAh g⁻¹) loss at various current rates (0.1, 0.2, 0.5, 1, 2 and 5 A g⁻¹), and nearly 100% discharge and charge capacity (1002 mAh g⁻¹) can be recovered once the rate is restored to the initial 0.1 A g⁻¹, demonstrating an excellent reversibility. However, the reversible capacity for GN is 701, 558, 429, 337, 289 and 236 mAh g⁻¹ at the current density of 0.1, 0.2, 0.5, 1, 2 and 5 A g⁻¹, which is 30% lower than for PPN/GN. The stable capacity of PPN/GN obtained at each current rate was also much higher than that of GN. The enhanced reversible capacity of PPN/GN over GN again suggests the successful composition of PPN on GN.

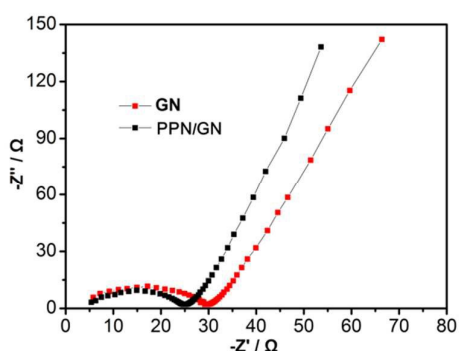


Fig. 7 Nyquist plots of the PPN/GN and GN electrodes

The electrochemical impedance spectroscopy (EIS) results for PPN/GN and GN are shown in the form of Nyquist plots in Fig. 8. Both EIS spectra show a straight line at the low frequency region, which represents the diffusion resistance of lithium. Both of them show a semicircle at the high-to-medium frequency region, representing the charge transfer resistance. It should be noted that the diameter of the semicircle for the PPN/GN electrodes (25 ohm) is somewhat smaller than that of thermal reduced GN (30 ohm), which revealed that the charge transfer resistance of the PPN/GN electrode is lower than that of GN electrode. In the low frequency region, PPN/GN showed a straight line that is close to the vertical axis, which indicates that the diffusion resistance is lower than GN. Both the lower charge transfer resistance and diffusion resistance of PPN/GN ascribe to the introduction of polarity polyphosphazene particles could fix the defects on GN sheets and benefic to fast Li⁺ diffusion and quick charge transfer at the interface between the electrolyte and the electrode.

Conclusions

Through a facile thermal polymerization of HCCP with GO, we have rationally prepared PPN/GN nanocomposites with stable and uniform structure. The HCCP reacted on GO sheets and in situ open-ring polymerized to well-defined polyphosphazene nanoparticles. The higher electron-coordination capability and stronger n-type behaviors of polyphosphazene nanoparticles afford more active sites for lithium storage and well separate the staking of graphene layers, which could effectively increase capacity and rate performance as LIBs anode. Meanwhile, the high molecular weight polyphosphazene nanoparticles firmly bonded on GN sheets through covalent bonds, which could effectively avoid the dissolution of active materials from electrode into electrolyte during cycling. Therefore, an excellent rechargeable capability (1002 mAh g⁻¹ at 100 mA g⁻¹) and rate performance (321 mAh g⁻¹ at 5 A g⁻¹ after 1200 cycles) as metal-free Li-ion battery anode could be achieved. All in all, the methodology described here would potentially afford a new way to develop high performance metal-free anode materials for LIBs.

Acknowledgements

This work is supported by the National Natural Science Foundation of China (Nos. 51303212, 21572269, 21302224, 51372277, 51572296); National Natural Science Foundation of Shandong Province (ZR2013BQ028, ZR2013EMQ013); The Fundamental Research Fund for the Central Universities (14CX02196A, 15CX08005A, 15CX05010A) and Qingdao Science and Technology Plan (15-9-1-108-jch).

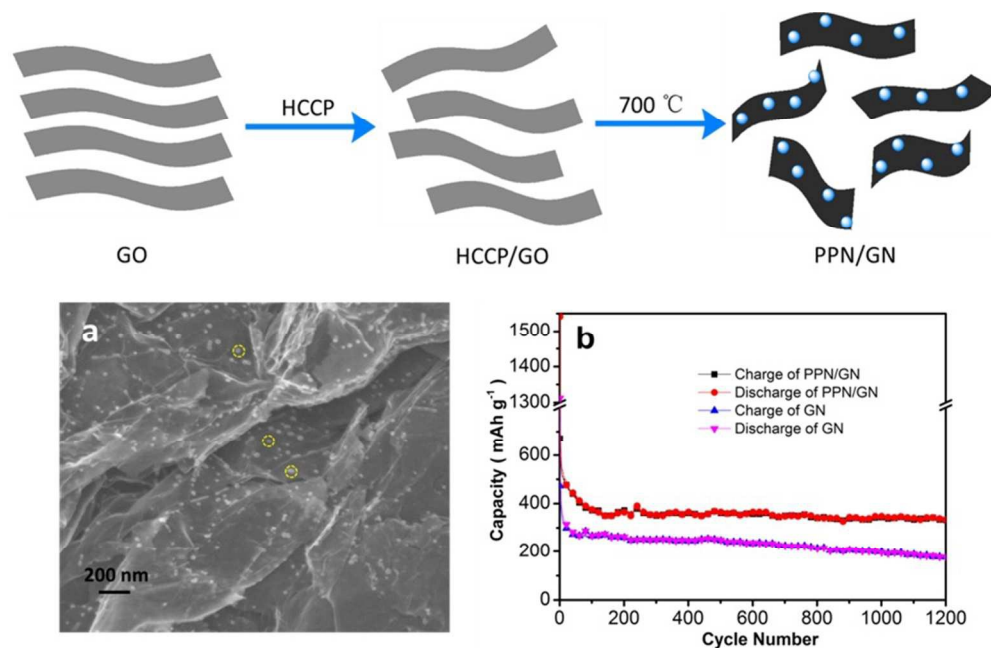
References

- B. Kang, G. Ceder. *Nature*, 2009, **458**, 190-193.
- C. Liu, F. Li, L. Ma, H. Chen. *Adv. Mater.*, 2010, **22**, E28-E62.
- Y. Fu, J. Zhu, C. Hu, X. Wu, X. Wang. *Nanoscale*, 2014, **6**, 12555-12564.
- Z. Wang, D. Luan, S. Madhavi, Y. Hu, X. Lou. *Energy Environ. Sci.*, 2012, **5**, 5252-5256.
- Y. Chiang. *Science*, 2010, **330**, 1485-1486.
- S. Jing, H. Jiang, Y. Hu, J. Shen, C. Li. *Adv. Funct. Mater*, 2015, **25**, 5395-5401.
- B. Guo, X. Wang, P. Fulvio, M. Chi, S. Mahurin, X. Sun, S. Dai. *Adv. Mater.*, 2011, **23**, 4661-4666.
- Z. Song, H. Zhan, Y. Zhou. *Angew. Chem. Int. Ed.*, 2010, **49**, 8444-8448.
- Y. Xue, B. Wu, L. Jiang, Y. Guo, L. Huang, J. Chen, J. Tan, D. Geng, B. Luo, W. Hu, G. Yu, Y. Liu. *J. Am. Chem. Soc.*, 2012, **134**, 11060-11063.
- P. Chen, T. Xiao, Y. Qian, S. Li, S. Yu. *Adv. Mater.*, 2013, **25**, 3192-3196.
- S. Vadahanambi, H. Chun, K. Jung, H. Park. *RSC Adv.*, 2016, **6**, 338112-38116.
- Y. Sun, J. Wu, J. Tian, J. Chao, R. Yang. *Electrochimica Acta*, 2015, **178**, 806-812.
- Y. Mao, H. Duan, B. Xu, L. Zhang, Y. Hu, C. Zhao, Z. Wang, Chen, Y. Yang. *Energy Environ. Sci.*, 2012, **5**, 7950-7955.
- X. Gu, C. Tong, C. Lai, J. Qiu, X. Huang, W. Yang, B. Wen, L. Liu, Y. Hou, S. Zhang. *J. Mater. Chem. A*, 2015, **3**, 16670-16678.
- L. Bulusheva, A. Okotrub, A. Kurennya, H. Zhang, H. Zhang, X. Chen, H. Song. *Carbon*, 2011, **49**, 4013-4023.
- L. Wang, Z. Gao, J. Chang, X. Liu, D. Wu, F. Xu, Y. Guo, K. Jiang. *ACS Appl. Mater. Interfaces*, 2015, **7**, 1-38.

ARTICLE

Journal Name

- 17 K. Xiao, Y. Liu, P. Hu, G. Yu, Y. Sun, D. Zhu. *J. Am. Chem. Soc.*, 2005, **127**, 8614-8617.
- 18 Y. Cho, H. Kim, H. Im, Y. Myung, G. Jung, C. Lee, J. Park, M. Park, J. Cho, H. Kang. *J. Phys. Chem. C*, 2011, **115**, 9451-9457.
- 19 C. Zhang, N. Mahmood, H. Yin, F. Liu, Y. Hou. *Adv. Mater.*, 2013, **25**, 4932-4937.
- 20 X. Ma, G. Ning, C. Qi, C. Xu, J. Gao. *ACS Appl. Mater. Interfaces*, 2014, **6**, 14415-14422.
- 21 G. Xu, L. Qi, B. Yu, L. Wen. *Solid State Ionics*, 2006, **177**, 305-309.
- 22 E. Dufek, M. Stone, D. Jamison, F. Stewart, K. Gering, L. Petkovic, A. Wilson, M. Harrup, H. Rolins. *J. Power Sources*, 2014, **267**, 347-355.
- 23 X. Wang, M. Wang, J. Fu, C. Zhang, Q. Xu. *J. Nanopart. Res.*, 2013, **15**, 557-560.
- 24 C. Zhang, R. Hao, H. Liao, Y. Hou. *Nano Energy*, 2013, 2(1):88-97.
- 25 M. Yu, A. Wang, Y. Wang, C. Li, G. Shi. *Nanoscale*, 2014, **6**, 11419-11424.
- 26 Z. Li, G. Wu, D. Liu, W. Wu, B. Jiang, J. Zheng, Y. Li, J. Li, M. Wu. *J. Mater. Chem. A*, 2014, **2**, 7471-7477.
- 27 Y. Wang, J. Mu, L. Li, L. Shi, W. Zhang, Z. Jiang. *High Perform. Polym.*, 2012, **24**, 229-236.
- 28 Z. Wang, P. Li, Y. Chen, J. He, J. Liu, W. Zhang, Y. Li. *J. Power Sources*, 2014, **263**, 246-251.
- 29 S. Niu, W. Lv, C. Zhang, F. Li, L. Tang, Y. He, B. Li, Q. Yang, F. Kang. *J. Mater. Chem. A*, 2015, **3**, 1-6.
- 30 Z. Li, G. Wu, S. Deng, S. Wang, Y. Wang, J. Zhou, S. Liu, W. Wu, M. Wu. *Chem. Eng. J.*, 2016, **283**, 1435-1442.
- 31 Z. Li, J. Zhou, R. Xu, S. Liu, Y. Wang, P. Li, W. Wu, M. Wu. *Chem. Eng. J.*, 2016, **287**, 516-522.
- 32 N. Mahmood, C. Zhang, J. Jiang, F. Liu, Y. Hou. *Chemistry*, 2013, **19**, 5183-5190.
- 33 N. Mahmood, C. Zhang, Y. Hou. *Small*, 2013, 9, 1321-1328.
- 34 S. Yan, K. Li, Z. Lin, H. Song, T. Jiang, J. Wu, Y. Shi. *RSC Adv.*, 2016, **6**, 32414-32421.
- 35 J. Dahn, T. Zheng, Y. Liu, J. Xue. *Science*, 1995, **270**, 590-593.



270x174mm (96 x 96 DPI)